JOURNAL OF MATERIALS SCIENCE: MATERIALS IN ELECTRONICS **16** (2005) 355–365

Creep rupture of lead-free Sn-3.5Ag and Sn-3.5Ag-0.5Cu solders

CHIH-KUANG LIN*, DE-YOU CHU
Department of Mechanical Engineering, National Central University, Chung-Li 32054, Taiwan
E-mail: t330014@cc.ncu.edu.tw

The aim of this study is to investigate the creep rupture behavior of lead-free Sn-3.5Ag and Sn-3.5Ag-0.5Cu solders at three temperatures ranging from room temperature (RT) to 90 °C, under a tensile stress range of $\sigma/E = 10^{-4}$ to 10^{-3}. The ultimate tensile strength (UTS) and creep resistance were found to be decreased with increasing temperature for each given lead-free solder. Both the binary and ternary Ag-containing alloys exhibited superior UTS and creep strength to the conventional Sn-37Pb solder at a similar temperature. Due to a more uniform distribution of eutectic phases and a larger volume fraction of intermetallic compounds (IMCs), the Sn-3.5Ag-0.5Cu alloy had greater UTS and creep strength than did the eutectic Sn-3.5Ag solder at each testing temperature. The stress exponents (n) of minimum strain rate ($\dot{\varepsilon}_{\min}$) were decreased from 7 and 9 at RT to 5 and 6 at 60 and 90 °C, for the binary and ternary lead-free alloys, respectively. Fractography analyses revealed typical rupture by the nucleation and growth of voids/microcracks at IMCs on the grain boundaries. Both Monkman-Grant and Larson-Miller relationships showed good results in estimating the rupture times under various combinations of applied stress and temperature. A model, using a term of applied stress normalized by Young's modulus, was proposed to correlate the rupture times at various temperatures and could explain the rupture time data reasonably well for the given two lead-free solders.
© *2005 Springer Science + Business Media, Inc.*

1. Introduction

Due to environmental and healthy concern, the allowable usage of lead will be decreased. The research and development of lead-free solders is being continuously and simultaneously carried out with the legislation against Pb-contained solders [1, 2]. The search of new lead-free solders with equivalent mechanical properties and microstructural stability to eutectic tin-lead solder is an urgent task. In the same time, the design of reliable joints with these newly developed lead-free solders needs to fully understand their mechanical properties and deformation mechanisms. The solder joints in electronic products play not only a role to interconnect the electronic components but also to ensure the structural reliability of the electronic packages. Therefore, it is very important to characterize the behavior of time-dependent, mechanical degradation of these lead-free solders so as to predict the lifetime of solder joints in electronic assemblies.

Failure of electronic package in service commonly occurs due to thermal mechanical fatigue (TMF) and creep at solder joints. Temperature fluctuations that result from power switching or environmental change could cause variation of strains imparted to the solder joints due to the different coefficients of thermal expansion (CTE) of the composed materials in the electronic package. As the solder is usually much softer than the joined components, the thermally induced strain is taken up primarily by the solder. Continued thermal cycling can then be expected to promote fatigue damage developed in the solder [3, 4]. However, service temperature changes seldom ramp up and then ramp down as rapidly as is found in typical thermal cycling test. Rather, the temperature is held constant for a period of time before changing. The service temperatures for electronic assemblies are usually located in the high homologous temperature ranges ($>0.5\ T_m$) of solders such that creep damage would take place during the hold period. In the case of solder which is constrained by harder surrounding materials, the thermal fatigue behavior may be best described as strain-controlled low-cycle fatigue accompanied with creep, or fatigue-creep interaction. Therefore, a thorough understanding of the creep behavior of solder alloys is of extreme importance to the designers of electronic assemblies.

Most studies of lead-free solders have been focused on Sn-based alloys. In particular, Sn-Ag alloys are expected to be a substitute for the eutectic Sn-37Pb solder,

*Author to whom all correspondence should be addressed.

TABLE I Nominal chemical composition of solder alloys tested (wt%)

Material	Sn	Ag	Cu	Pb	Sb	Bi	Fe	As
Sn-37Pb	Bal.	–	0.008	36.96	0.014	0.008	0.003	0.003
Sn-3.5Ag	Bal.	3.49	0.008	0.021	0.014	0.007	0.003	0.004
Sn-3.5Ag-0.5Cu	Bal.	3.50	0.501	0.015	0.014	0.008	0.003	0.003

because they have better mechanical properties (ductility, creep resistance and thermal resistance) than the Sn-Pb solder [5]. In addition, Sn-Ag-Cu alloys are also considered as another replacement, because they have lower melting temperatures and good wettability compared with the eutectic Sn-3.5Ag alloy. Creep is one of the most important deformation mechanisms for solder joints in electronic products for long-term use at high homologous temperatures. Although there have been several creep studies on Sn-Ag and Sn-Ag-Cu alloys in the literature [6–18], studies related to the temperature effects on the creep behavior and lifetime prediction methodology in such lead-free solders were quite limited. Hence, the purpose of this study was to investigate and quantify the creep properties of two promising lead-free solders, Sn-3.5Ag and Sn-3.5Ag-0.5 Cu, at various environmental temperatures so as to provide important and helpful information for the electronic packaging designers. The effect of addition of 0.5% Cu on the microstructure and creep resistance of Sn-3.5Ag solder was studied at three given temperatures. In addition, the creep behavior of Sn-37Pb eutectic solder at room temperature was also investigated in order to make a comparison with the selected lead-free solders.

2. Experimental procedures

The eutectic Sn-37Pb, Sn-3.5Ag, and near-eutectic Sn-3.5Ag-0.5Cu solder alloys used in the current study were supplied by a local vendor[1] in the form of extruded round bars. The chemical compositions of the three materials are given in Table I. Axial smooth-surface specimens with a uniform cylindrical gage section of 8 mm in diameter and 48 mm in length were used in both tensile and creep tests. Tensile tests were carried out on a commercial closed-loop servo-hydraulic test machine and conducted as per ASTM E8M-98 under stroke control with a strain rate of 10^{-3} s^{-1} at room temperature (RT), 60 and 90 °C. Specimens were heated to the expected temperatures by a heating strip. A commercial direct-contact extensometer with a 25-mm gage length was used to measure the tensile strain.

The creep tests were performed in accordance with ASTM E139-96 under constant load at RT, 60 and 90 °C. These testing temperatures correspond to a range of about 0.6–0.74 T_m (homologous temperature) for the two given lead-free solders. A direct-load creep testing machine was used to perform the constant-load creep tests with application of various load weights as the loading source. With a proper selection of load weights, the lifetime of creep test at each temperature condition fell in the range of several to about one thousand hours. The same extensometer used in tensile tests was employed to measure the creep strain. To avoid the direct contact between the knives of the extensometer and the surface of soft solders, epoxy resin bumps were glued on the contacting areas of the specimen to reduce the damage generated by the knives of extensometer. Note that both tensile and creep tests for the eutectic Sn-37Pb alloy were only conducted at RT (∼0.65 T_m) for comparison purpose. Scanning electron microscopy (SEM) was used for characterization of microstructure, fracture surface morphology and surface creep damages.

[1] Redsun Metal Industrial Co., Ltd., Chung-Li, Taiwan.

3. Results and discussion

3.1. Microstructure and tensile properties

SEM micrographs of the microstructure in the given two lead-free and Sn-37Pb solders are shown in Fig. 1. The microstructure of the eutectic Sn-3.5Ag alloy is shown in Fig. 1(a), in which the dark areas are the eutectic phases and the light areas consist of fine intermetallic compounds (IMCs) of Ag_3Sn dispersed in the β-Sn matrix. The eutectic composition in Sn-Ag-Cu system was determined as Sn-3.5 wt%Ag-0.9 wt%Cu by Loomans and Fine [19] or Sn-3.66 wt%Ag-0.91 wt%Cu by Moon *et al.* [20]. Hence, the composition of the Sn-3.5Ag-0.5Cu solder used in the current study is very close to the eutectic one. As shown in Fig. 1(b), the given near-eutectic Sn-3.5Ag-0.5Cu alloy has a similar microstructure to that in the Sn-3.5Ag alloy, while the light areas are β-Sn matrix decorated with fine Ag_3Sn and Cu_6Sn_5 IMCs. The SEM micrograph of the microstructure for the eutectic Sn-37Pb solder alloy is shown in Fig. 1(c) where the dark and light regions are the eutectic and primary β-Sn phases, respectively.

The tensile properties for the given three alloys are summarized in Tables II–IV. At RT, the Sn-37Pb solder

TABLE II Mechanical properties of Sn-37Pb at RT

Temperature (°C)	Elastic modulus (GPa)	Ultimate tensile strength (MPa)	Elongation (in 25 mm) (%)
RT	24	26.3	>200

TABLE III Mechanical properties of Sn-3.5Ag at different temperatures

Temperature (°C)	Elastic modulus (GPa)	Ultimate tensile strength (MPa)	Elongation (in 25 mm) (%)
RT	45	46.0	68.8
60	30	30.0	78.1
90	22	24.8	79.4

TABLE IV Mechanical properties of Sn-3.5Ag-0.5Cu at different temperatures

Temperature (°C)	Elastic modulus (GPa)	Ultimate tensile strength (MPa)	Elongation (in 25 mm) (%)
RT	42	47.8	71.2
60	26	31.2	80.3
90	16	25.1	86.2

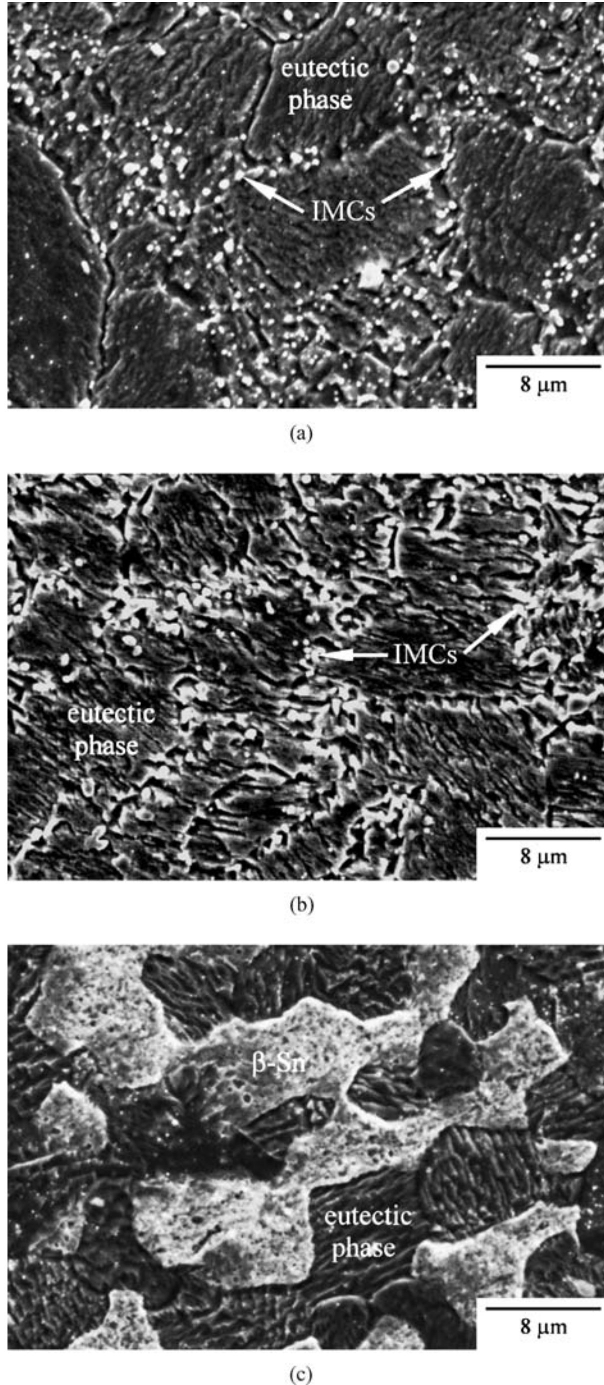

Figure 1 SEM micrographs of microstructure in (a) Sn-3.5Ag, (b) Sn-3.5Ag-0.5Cu and (c) Sn-37Pb.

has the lowest elastic modulus of 24 GPa and the Sn-3.5Ag alloy has the highest one of 45 GPa, while the Sn-3.5Ag-0.5Cu alloy stands in between and has a value of 42 GPa. Both lead-free solders have greater ultimate tensile strength (UTS) than does the Pb-containing one at room temperature. This is due to a dispersion-strengthening effect of the fine IMCs in the two lead free solders. The UTS of the Sn-3.5Ag-0.5Cu alloy is higher than that of the Sn-3.5Ag alloy at each testing temperature. The higher UTS of the Sn-3.5Ag-0.5Cu alloy could be attributed to an addition of 0.5Cu in the Sn-3.5Ag alloy which could form a more uniform distribution of eutectic phases and a larger volume fraction of IMCs than the Sn-3.5Ag alloy. In addition, it is also seen that the Sn-3.5Ag-0.5Cu alloy has a better ductility than the Sn-3.5Ag solder at each given temperature.

3.2. Creep curves

Creep curves of the Sn-3.5Ag, Sn-3.5Ag-0.5Cu and Sn-37Pb at RT are presented in Fig. 2. It is seen in these materials the primary stage was fairly short such that the secondary creep stage showed up right after loading. This indicates that the strain hardening in the primary creep was rapidly recovered at such a high temperature ($>0.5\ T_m$) leading to a balance between the hardening and recovery rate. Similar characteristics in creep curves can also be observed at 60 and 90 °C for the two lead-free solders. A typical example of the normalized creep curves (where the creep strain and lifetime were normalized with respect to rupture strain and rupture time, respectively) for these cases is shown in Fig. 3. The steady-state deformation typically occupied about 30–50% of the entire creep life in the given three solder alloys at each testing temperature.

Minimum creep (strain) rates were determined from the above creep curves as functions of stress and temperature for each given alloy. Log-log plots of the minimum strain rate as functions of applied stress for the given solders at various testing temperatures are given in Fig. 4. A simplified form of Dorn equation [21] was used to correlate the minimum creep rate and applied stress:

$$\dot{\varepsilon}_{\min} = A\sigma^n \exp\left(\frac{-Q}{RT}\right) \qquad (1)$$

where $\dot{\varepsilon}_{\min}$ is the minimum strain rate, A is a material-dependent constant, σ is the applied stress, n is the stress exponent, Q is the activation energy, R is the universal gas constant, and T is the absolute temperature. In Fig. 4, the slope of each fitted straight line represents the value of stress exponent, n, for each solder alloy at a given testing temperature. It has been recognized that the value of stress exponent is an index of creep deformation mechanism. According to the deformation mechanism map and previous studies [11, 22–24], the predominant creep mechanism corresponding to the stress exponent values of 5 (Sn-3.5Ag) and 6 (Sn-3.5Ag-0.5Cu) for the two lead-free solders at 60 and 90 °C was, presumably, a type of dislocation creep of lattice-diffusion-controlled dislocation climb coupled with a dispersion-strengthening mechanism. However, higher values of stress exponent were observed for these two lead-free solders at RT ($n = 7$ for Sn-3.5Ag and $n = 9$ for Sn-3.5Ag-0.5Cu) implying a creep deformation mechanism related to and dominated by a dispersion-strengthening mechanism, such as Orowan mechanism [8, 11, 12, 14]. Larger n values

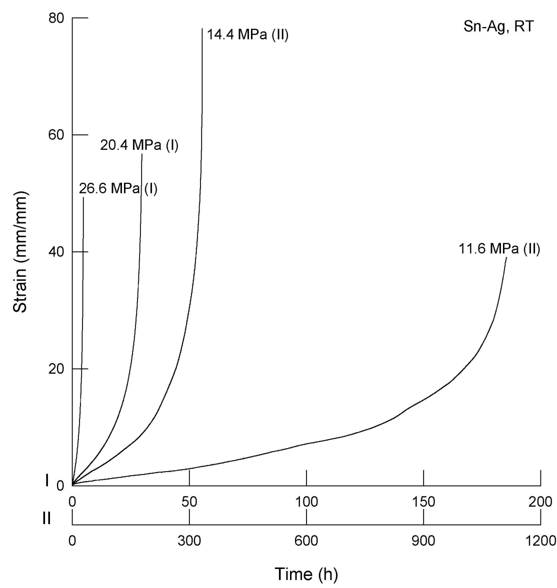

(a)

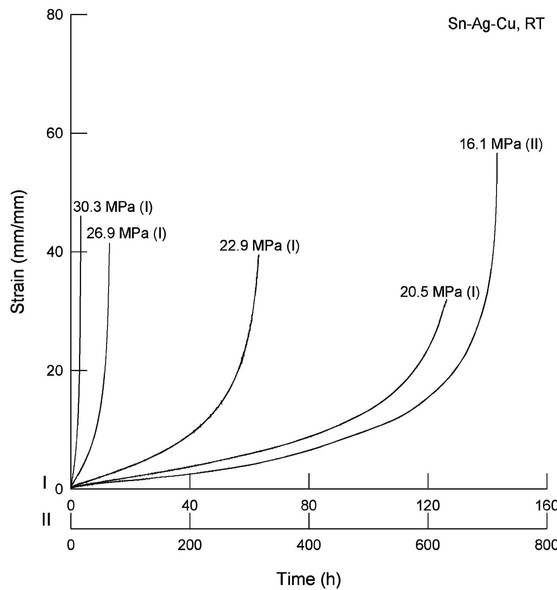

(b)

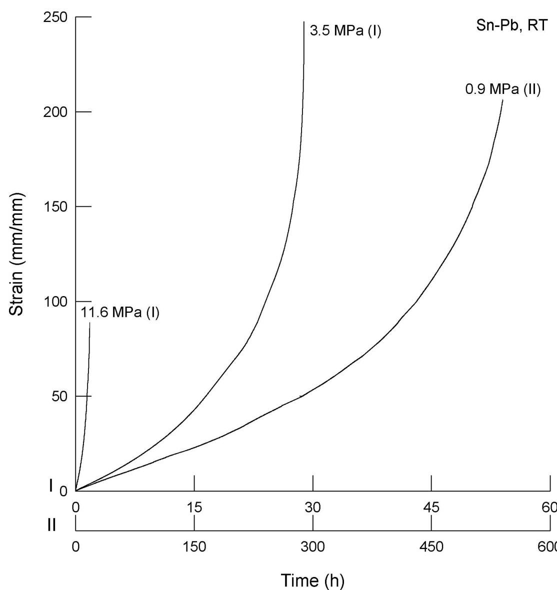

(c)

Figure 2 Typical creep curves at RT for (a) Sn-3.5Ag, (b) Sn-3.5Ag-0.5Cu and (c) Sn-37Pb solder alloys. (Note that two scales were used in the abscissa.)

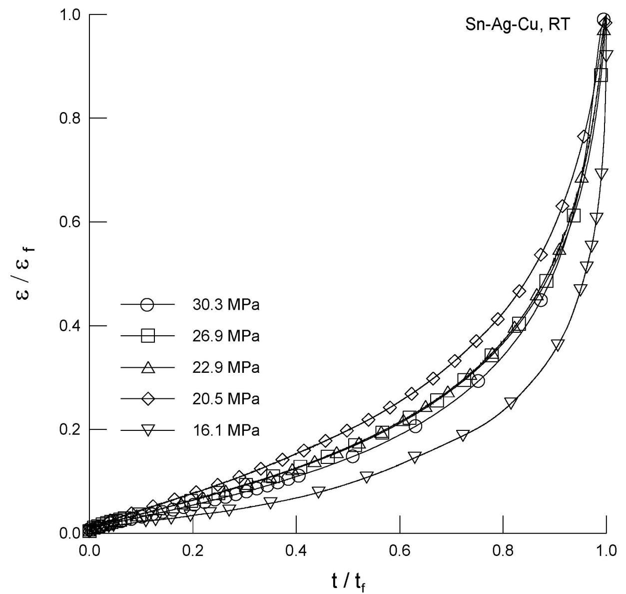

Figure 3 Normalized creep curves at RT for Sn-3.5Ag-0.5Cu solder alloy.

observed at RT than at 60 and 90 °C for the two given lead-free alloys indicate the dispersion-strengthening effect was more effective at RT than at high temperatures. The stress exponent of $n = 2$ for the given conventional Sn-37Pb alloy at RT indicates a superplastic deformation mechanism controlled by grain boundary sliding [23–25].

The n value was generally increased with increasing creep strength and decreased at higher temperatures [17, 26]. The measured n values shown in Fig. 4 show the same tendencies. Accordingly, the Sn-3.5Ag-0.5Cu alloy has the greatest creep resistance, followed by the Sn-3.5Ag and then the Sn-37Pb. This tendency is also seen in the creep-rupture time results. Comparison of creep strength for the given solders was also made by plotting applied stress as functions of rupture time at various testing temperatures, as shown in Fig. 5. It is clearly seen in Figs. 4 and 5 that the creep strength of the conventional Sn-37Pb solder at RT is much less than that of the given two lead-free ones. For a given stress at RT, the minimum strain rate of the Pb-containing alloy is greater by more than two orders of magnitude than those of the two lead-free ones such that the corresponding rupture time is also shorter by more than two orders of magnitude. However, intrinsic creep resistance for alloys with different melting temperatures should be made a comparison at similar homologous temperatures. In this regard, by comparing the creep data of the two lead-free solders at 60 °C ($\sim$0.67 T_m) with those of the Sn-37 Pb at RT ($\sim$0.65 T_m), the two lead-free solders still show lower creep rates and longer rupture times under a similar (or very close) homologous temperature. This once again confirms the better creep rupture strength of the two lead-free solders over the eutectic Sn-Pb one. The inherent superiority of the given two lead-free solders to the Sn-37Pb one in creep strength can be attributed to a dispersion-strengthening effect of the fine IMCs in the two lead free solders as described in the previous section.

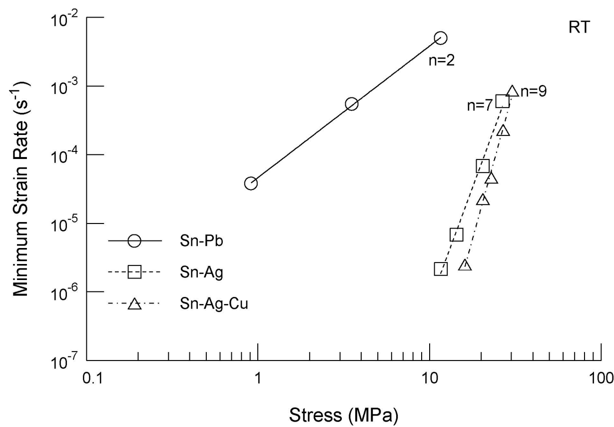

(a)

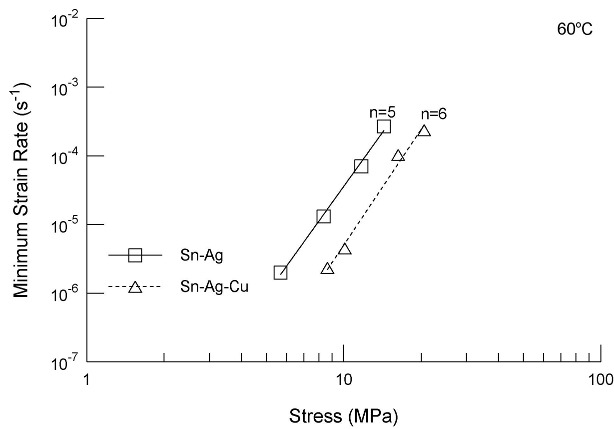

(b)

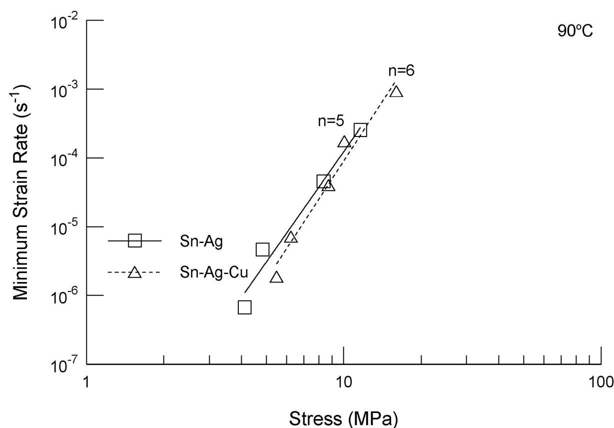

(c)

Figure 4 The relationship between minimum creep rate and applied stress at (a) RT, (b) 60 °C and (c) 90 °C.

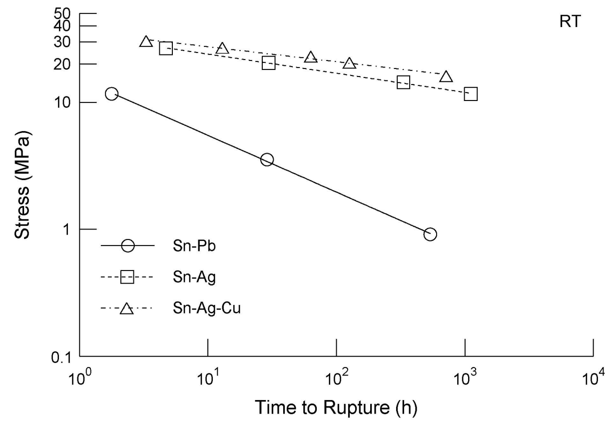

(a)

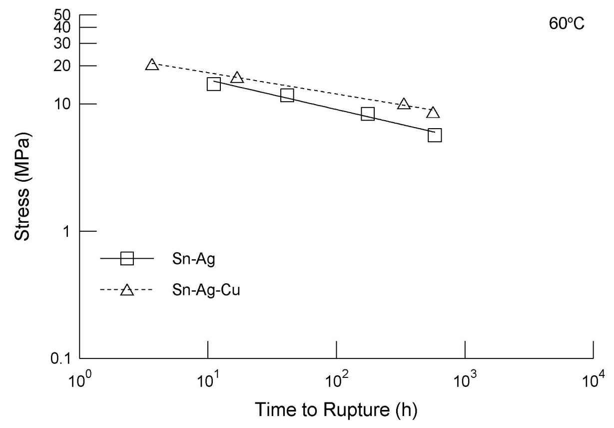

(b)

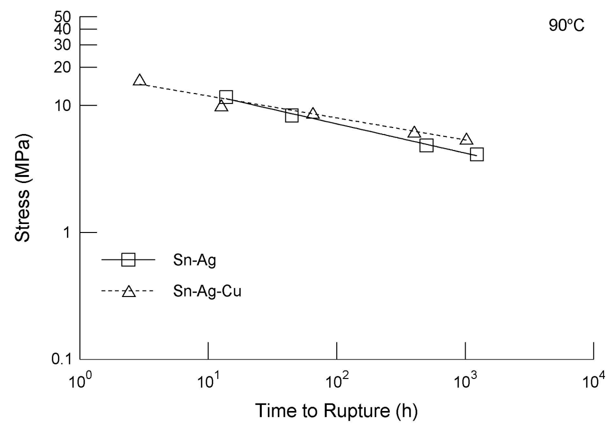

(c)

Figure 5 Applied stress vs. rupture time at (a) RT, (b) 60 °C and (c) 90 °C.

The Sn-3.5Ag-0.5Cu solder has the greatest creep strength among the given three alloys as it shows the highest value of stress exponent, lowest minimum creep rate, and longest rupture time at a given stress and temperature. The greater creep resistance of the ternary Sn-3.5Ag-0.5Cu solder over the binary Sn-3.5Ag one at each given temperature could be attributed to an addition of 0.5% Cu in the eutectic Sn-Ag alloy which caused a more uniform distribution of eutectic phases as well as a larger volume fraction of IMCs in the matrix, as shown in Fig. 1. Apparently, the addition 0.5 wt% Cu in the Sn-3.5Ag is an effective approach for increasing the creep and rupture strength of the lead-free Sn-3.5Ag solder.

3.3. Effect of temperature on creep behavior

The effect of temperature on the creep strength for Sn-3.5Ag and Sn-3.5Ag-0.5Cu solder alloys is presented in Fig. 6 by plotting applied stresses as a function of rupture time at various temperatures. As expected, the creep resistance for the given two lead-free solders was decreased with an increase in temperature. Fig. 7 shows the effect of temperature on the minimum strain rate for the given two lead-free solders by plotting the minimum strain rate against the reciprocal temperature in natural logarithmic-linear coordinates with various combinations of applied stress and temperature. The value of activation energy, Q, in Equation 1 can be determined from the slope of the fitted straight lines for certain

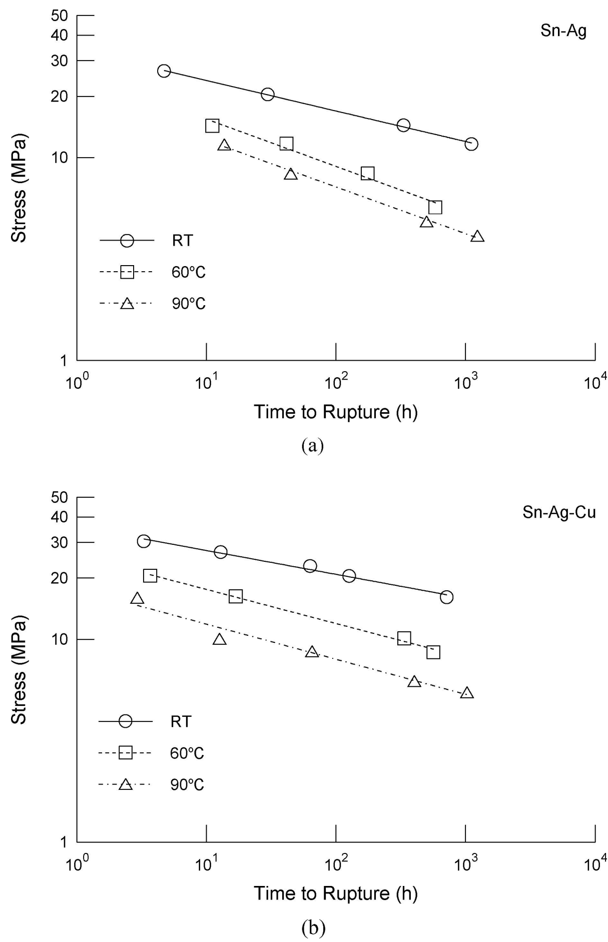

Figure 6 Applied stress vs. rupture time at various temperatures for (a) Sn-3.5Ag and (b) Sn-3.5Ag-0.5Cu alloys.

stresses, as shown in Fig. 7. The activation energy for the Sn-3.5Ag and Sn-3.5Ag-0.5Cu solders at various given stresses were determined to be in the range from 41.8 to 86.4 kJ/mol and 55.3 to 123.0 kJ/mol, respectively. The measured activation energies were found to be stress dependent for each given lead-free alloy. However, no clear trend between the activation energy and stress level could be found due to a limited number of data points, as there were only two data points for some stress levels.

From the overall comparison of these measured Q values, the Sn-3.5Ag-0.5Cu, presumably, has a greater Q value than does the Sn-3.5Ag. For example, at a stress level around 8.3 or 8.6 MPa, the Q value for Sn-3.5Ag-0.5Cu is 95.5 kJ/mol and markedly larger than the one of 41.8 kJ/mol for Sn-3.5Ag. For the two cases with three data points in each fitted curve, Sn-3.5Ag-0.5Cu has a Q value of 82.3 kJ/mol at a stress of 16.1 MPa while Sn-3.5Ag has a Q value of 67.0 MPa at a stress of 11.6 MPa. A greater activation energy of creep for Sn-3.5Ag-0.5Cu solder is consistent with its greater creep resistance, as compared to Sn-3.5Ag. This suggests that energy barrier for creep in the Sn-3.5Ag-0.5Cu solder is raised and dislocation motion is hindered to a greater extent by a larger volume fraction of IMCs over the Sn-3.5Ag. The activation energy of creep for Sn-3.5Ag at various uniaxial tensile stresses was found to be in the range from 75 to 82 kJ/mol under stresses 16 to 20 MPa by Wu *et al.* [9] and Huang *et al.* [16], and 79.5 kJ/mol

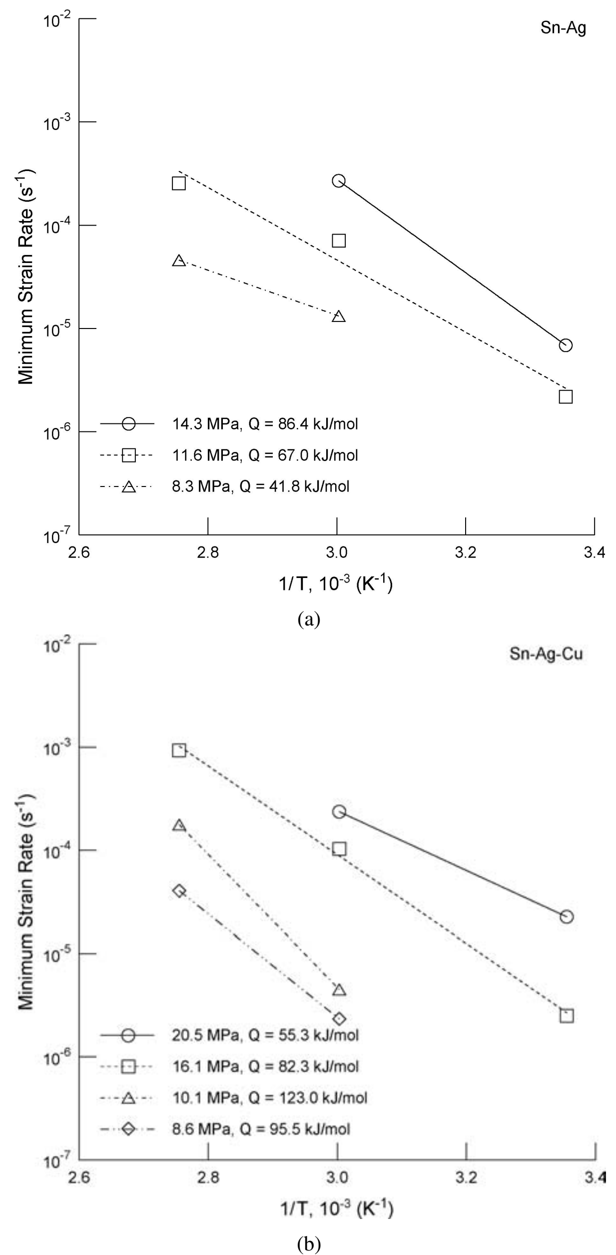

Figure 7 Minimum strain rates for (a) Sn-3.5Ag and (b) Sn-3.5Ag-0.5Cu solder alloys at various temperatures under certain stresses.

under stresses from 10 to 22 MPa by Mavoori *et al.* [18]. Apparently, the measured Q values of Sn-3.5Ag in the current study are consistent with other studies. However, no such data in uniaxial tensile creep could be found for the alloy Sn-3.5Ag-0.5Cu in literature to make a comparison.

3.4. Parametric models for rupture time

For design purpose, it would be very helpful if any methods are available for correlating and extrapolating creep-rupture data such that the rupture time at various combinations of stress and temperature can be accurately predicted. Two parametric models, Monkman-Grant [27] and Larson-Miller [28] relationships, were adopted in the current study to correlate the rupture time data for the given two lead-free solders under the given testing conditions. The former used the minimum strain rate as a key variable to assess the rupture time while

the latter used applied stress and temperature as primary parameters. Monkman and Grant [27] observed that the rupture time, t_f, in long term creep test could be related to the minimum strain rate by a power law function:

$$\dot{\varepsilon}_{\min} t_f^m = C_{MG} \quad (2)$$

where the exponent m and constant C_{MG} are material dependent. The constant C_{MG} usually depends on temperature. The practical advantage of the Monkman-Grant rule is that the minimum strain rate can be measured early in a creep test so as to predict a long life case. Provided the value of C_{MG} can be determined in short-term tests, the lifetime of a long-term test can be predicted once the minimum strain rate has been established.

The results in applying this empirical formulation to the obtained creep-rupture data for the given two lead-free solder alloys and testing conditions are presented in Tables V and VI. Note that in Tables V and VI the fitted Monkman-Grant expressions of individual and all testing temperatures are included for each alloy. As seen in Tables V and VI, for each alloy, the Monkman-Grant expressions in various testing temperatures are quite comparable and it is reasonable to fit all the data from various temperatures by a single Monkman-Grant expression, as shown in Fig. 8. As shown in Fig. 8, for the given ranges of stress and temperature, each lead-free alloy adheres quite well to a single Monkman-Grant relationship. The Monkman-Grant expressions for each fitted straight line in Fig. 8 are also presented in Tables V and VI designated as "All" in the temperature column. These two equations are given again as follows:

$$\dot{\varepsilon}_{\min} t_f^{1.14} = 4.1 \times 10^{-3} \quad \text{for Sn-3.5Ag} \quad (3)$$

$$\dot{\varepsilon}_{\min} t_f^{1.02} = 2.2 \times 10^{-3} \quad \text{for Sn-3.5Ag-0.5Cu} \quad (4)$$

The high values of the correlation coefficient ($r^2 =$ 0.98 and 0.97) for these two fitted expressions indicate an excellent applicability of the Monkman-Grant relationship to correlate the rupture time with minimum creep rate for the given binary and ternary Ag-bearing alloys. In this regard, it may be reasonable to say that the Monkman-Grant relationship for each given lead-free solder alloy is approximately independent of temperature over the range of given testing conditions. Thus, we can estimate rupture time from the minimum creep rate or vice versa, regardless of temperature, as the obtained C_{MG} values in these two equations have already covered all the given testing temperatures and the temperature effect has been averaged through the fitting process. Therefore, these two expressions could serve as useful tools to predict the rupture time for the given two lead-free solders at various combinations of stress and temperature. Note the fact that rupture time correlates well with minimum creep rate implies cavity formation and growth is basic to the intergranular creep fracture process [29]. This is supported by the fractography observations, which is to be discussed in next section.

In addition to Monkman-Grant rule, another creep life relationship, Larson-Miller relationship [28], which is similar in principle but different in its functional form is also applied in this study to correlate the rupture time with applied stress and temperature. In 1952, Larson and Miller [28] assumed the following relation between creep lifetime, applied stress and temperature:

$$P_{LM} = T(C_{LM} + \log t_f) \quad (5)$$

TABLE V Monkman-Grant expressions for Sn-3.5Ag solder

Temperature	Equation	Correlation coefficient (r^2)
RT	$\dot{\varepsilon}_{\min} t_f^{1.02} = 2.6 \times 10^{-3}$	0.99
60 °C	$\dot{\varepsilon}_{\min} t_f^{1.22} = 5.9 \times 10^{-3}$	0.99
90 °C	$\dot{\varepsilon}_{\min} t_f^{1.23} = 6.1 \times 10^{-3}$	0.98
All	$\dot{\varepsilon}_{\min} t_f^{1.14} = 4.1 \times 10^{-3}$	0.98

TABLE VI Monkman-Grant expressions for Sn-3.5Ag-0.5Cu solder

Temperature	Equation	Correlation coefficient (r^2)
RT	$\dot{\varepsilon}_{\min} t_f^{1.07} = 3.5 \times 10^{-3}$	0.99
60 °C	$\dot{\varepsilon}_{\min} t_f^{0.94} = 1.0 \times 10^{-3}$	0.99
90 °C	$\dot{\varepsilon}_{\min} t_f^{1.02} = 2.7 \times 10^{-3}$	0.99
All	$\dot{\varepsilon}_{\min} t_f^{1.02} = 2.2 \times 10^{-3}$	0.97

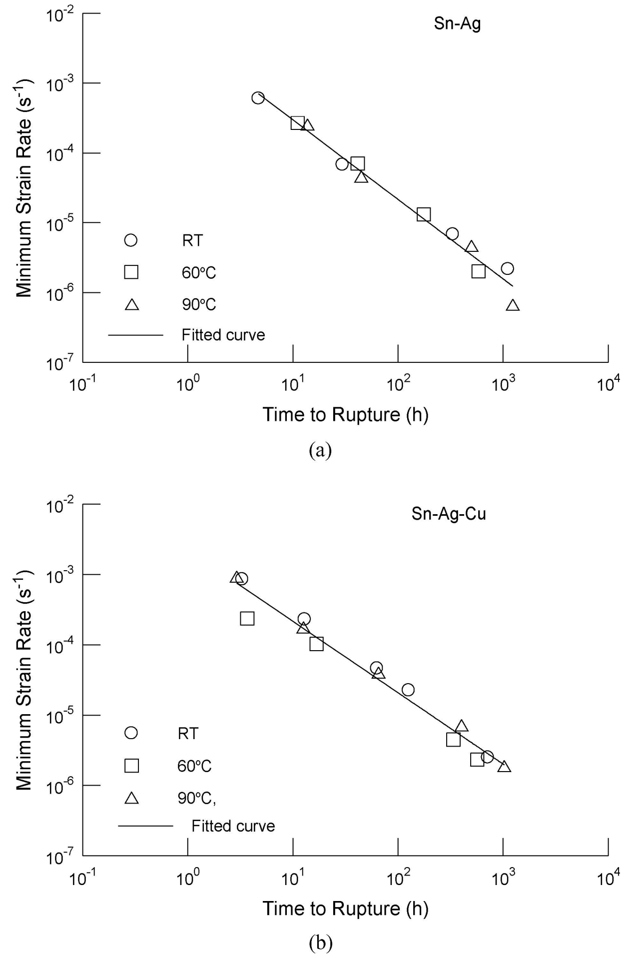

Figure 8 Monkman-Grant plots of all measured data for (a) Sn-3.5Ag and (b) Sn-3.5Ag-0.5Cu alloys.

where P_{LM} is the Larson-Miller parameter and is a function of applied stress, T is temperature in Kelvin and t_f is creep rupture time in hours. The value of C_{LM} can be obtained by extrapolating an intercept of log $t_f = -C_{LM}$ on a plot of log t_f versus 1/T at $1/T = 0$. In this way, the extrapolating values of C_{LM} at select stresses applied in all the given temperatures for the Sn-3.5Ag and Sn-3.5Ag-0.5Cu solders were determined as about 8 and 11, respectively. Values of constant C_{LM} for steels and other engineering metals are often around 20. Once C_{LM} is obtained, Equation 5 become the following expressions for the given two lead-free solders.

$$P_{LM} = T(8 + \log t_f) \quad \text{for Sn-3.5Ag} \tag{6}$$

$$P_{LM} = T(11 + \log t_f) \quad \text{for Sn-3.5Ag-0.5Cu} \tag{7}$$

After the value of constant C_{LM} was determined, values of P_{LM} for each given stress level and lead-free alloy could be determined from the stress-life data using Equations 6 and 7. The obtained P_{LM} values were then plotted against stress, as shown in Fig. 9. It is seen in Fig. 9 that the obtained Larson-Miller parameters and applied stresses could be well correlated by a linear relation for the given two lead-free solders at various temperatures. The best-fitted curves with a linear regression analysis indicate the following relations:

$$P_{LM} = -59\sigma + 4.0 \times 10^3 \quad \text{for Sn-3.5Ag} \tag{8}$$

$$P_{LM} = -60\sigma + 5.1 \times 10^3 \quad \text{for Sn-3.5Ag-0.5Cu} \tag{9}$$

The values of correlation coefficient (r^2) for Equations 8 and 9 are of 0.91 and 0.95, respectively. By using Equations 6 through 9, creep rupture time can be predicted for these two lead-free solders at various combinations of stress and temperature.

As discussed above, the application of these two models to analyze the experimental data of rupture time was quite successful for the given two lead-free solder alloys. This means that we can either use minimum creep rate (through Monkman-Grant expression) or applied stress level and temperature (through Larson-Miller relationship) as an variable to estimate the creep rupture time for Sn-3.5Ag and Sn-3.5Ag-0.5Cu at a variety of stress-temperature combinations. In order to estimate the rupture time by a more convenient form and accessible parameters, it is proposed in the present work to correlate the rupture time with the applied stress normalized by Young's modulus to correct the temperature dependence. The results in Fig. 6 are rearranged by plotting normalized applied stress as a function of rupture time and shown in Fig. 10. Note that the Young's moduli given in Tables III and IV for each lead-free alloy at various temperatures were used to normalize the applied stress at each corresponding testing temperature. As shown in Fig. 10, through such a normalization, the initially, distinctly distanced data points in Fig. 6 now become quite closer indicating an independence of temperature in normalized stress for each alloy. In other words, the intrinsic temperature dependence of

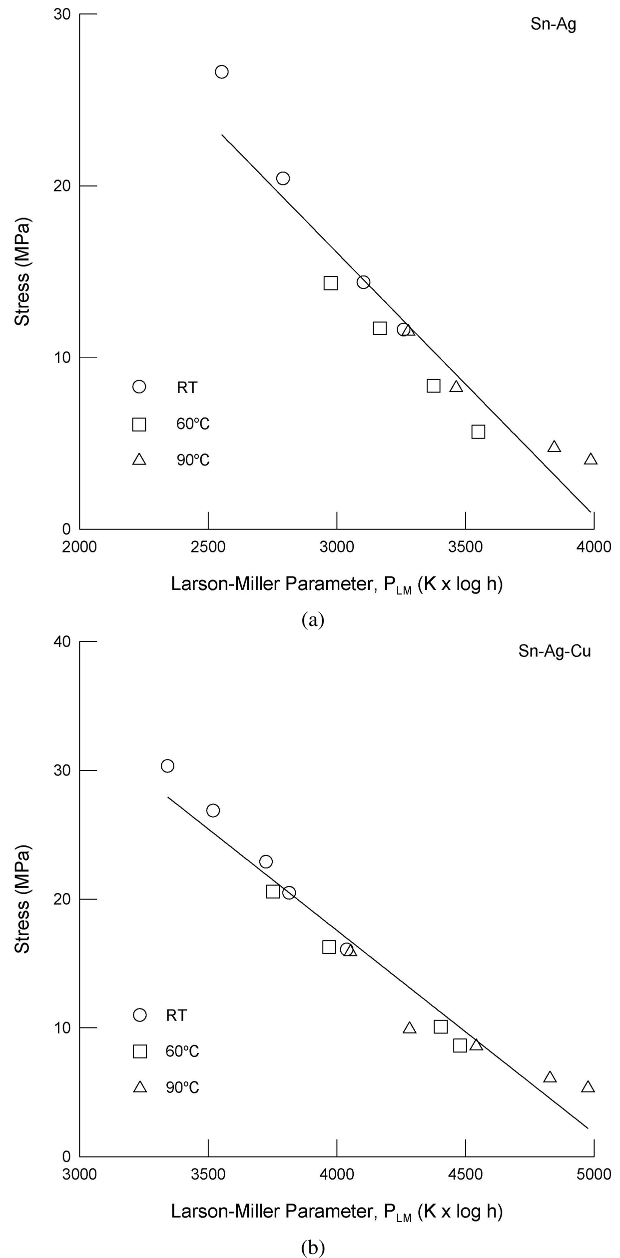

Figure 9 Master curve of Larson-Miller parameter for (a) Sn-3.5Ag and (b) Sn-3.5Ag-0.5Cu solder alloys.

rupture time is implied in the Young's modulus term. The data points shown in Fig. 10 for each alloy could be well correlated by a simple power law $(\frac{\sigma}{E})t_f^{m'} = D$, where m' and D are constants. The obtained best-fit curves for each alloy are presented as follows:

$$\left(\frac{\sigma}{E}\right)t_f^{0.196} = 8.2 \times 10^{-4} \quad \text{for Sn-3.5Ag} \tag{10}$$

$$\left(\frac{\sigma}{E}\right)t_f^{0.155} = 9.9 \times 10^{-4} \quad \text{for Sn-3.5Ag-0.5Cu} \tag{11}$$

The high values of correlation coefficient for Equations 10 and 11, $r^2 = 0.90$ and 0.95, respectively, suggest that the proposed normalized stress, (σ/E), can be used to estimate the rupture time in a more convenient way compared with the Monkman-Grant and Larson-Miller relationships when considering the temperature effect.

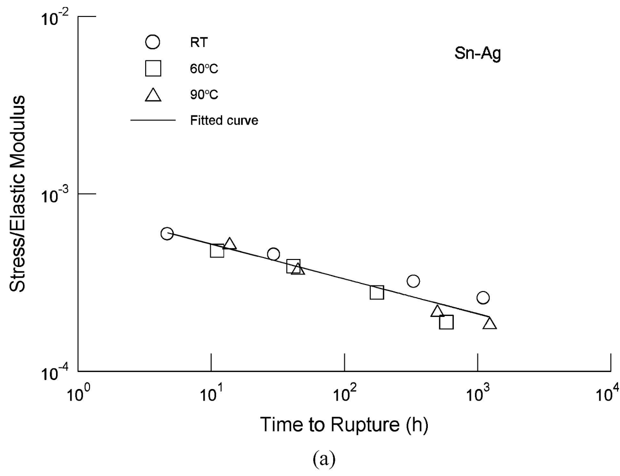

(a)

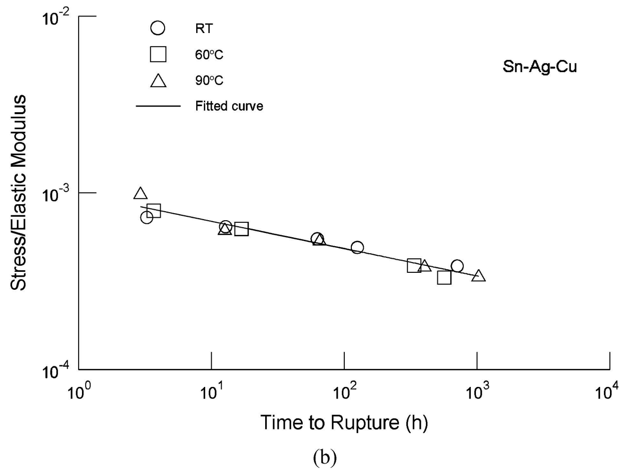

(b)

Figure 10 Normalized stress vs. rupture time for (a) Sn-3.5Ag and (b) Sn-3.5Ag-0.5Cu alloys.

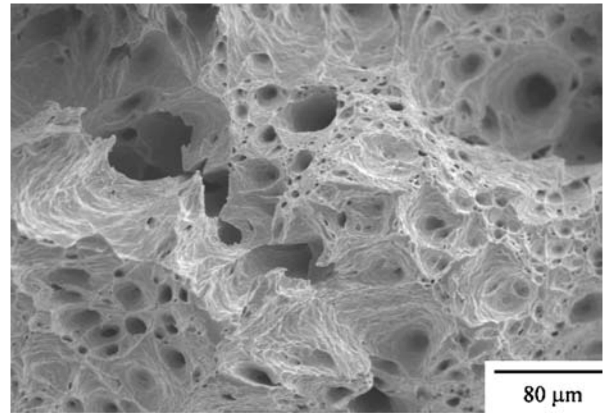

(a)

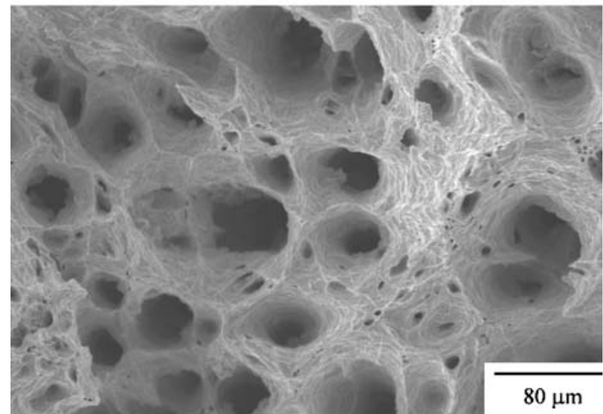

(b)

Figure 11 SEM micrographs of creep fracture surface in the Sn-3.5Ag-0.5Cu alloy at (a) RT and (b) 90 °C.

3.5. Fractography analyses

Fractography analyses of the crept specimens for all the given lead-free solder alloys indicated the final fracture was a ductile type and accompanied by considerable necking. Fig. 11 shows examples of SEM micrograph of creep fracture surface for the Sn-3.5Ag-0.5Cu solder at RT and 90 °C. Similar features of fracture surface were also observed in the Sn-3.5Ag alloy. A typical ductile-material type of void coalescence feature was observed in these micrographs. However, the number of deeper void was greater at 90 °C, as shown in Fig. 11(b). This might be attributed to easier formation and faster growth of voids at dispersed IMCs at a higher temperature. It was reported that the decohesion and nucleation of voids at the IMCs was caused by an incompatibility of creep flow between the matrix and IMC [12]. These voids situated on grain boundaries would coalesce and link up to become microcracks during creep process.

In addition to analyzing the features of fracture surface, circumferential surfaces within gage section of the crept specimens were also examined by SEM for the given lead-free solders to seek any possible evidence of creep damages. From such observations, voids and microcracks were readily seen along grain boundaries (GBs) in the given lead-free solder alloys, as exemplified in Fig. 12. It was reported that voids could be formed at the early stage of creep deformation and then lasting for a long period of time until the final fracture [6, 7]. The presence of these voids and microcracks provided evidence for the viewpoint that the creep mechanisms for the given lead-free solders and testing conditions were related to the strengthening IMC particles, as described above. As indicated by arrows in Fig. 12, the voids formed at IMCs on GBs would grow and coalesce to become microcracks. As suggested by earlier works [6, 7, 29], the formation of GB voids at hard, dispersed precipitates in dispersion-strengthened alloys is a process accommodating GB sliding, together with diffusional creep. Once being created, the intergranular voids and microcracks serve as vacancy sinks in the process of stress relaxation [6, 7]. As a result, they grow along GB by diffusive mass transport, which is a kinetic process driven by a continuous creep deformation inside the grain [6, 7]. In the current study, where the given testing conditions can be classified as high homologous temperatures (0.6–0.74 T_m) together with high normalized stresses ($10^{-4} < \sigma/E < 10^{-3}$), the continuous creep deformation is likely to be a dislocation creep mechanism coupled with a dispersion-strengthening one, as indicated by the measured values of stress exponent. The voids/microcracks grow and coalesce, through the ductile failure of microcracks, and then the final fracture was a ductile type, as shown in Fig. 11.

Based on the SEM observations and the measured values of stress exponent for the given testing conditions, it is considered that creep rupture for the given two lead-free solder alloys occurred by nucleation of

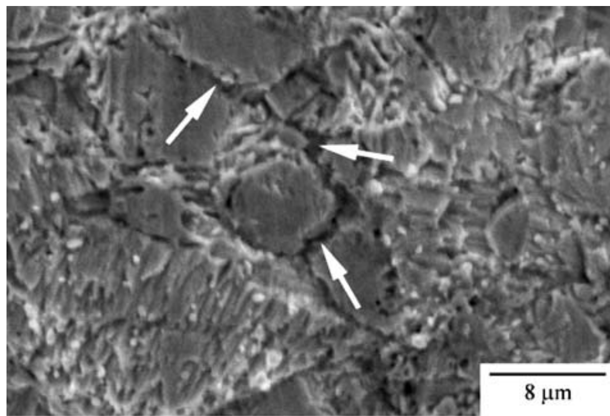

(a)

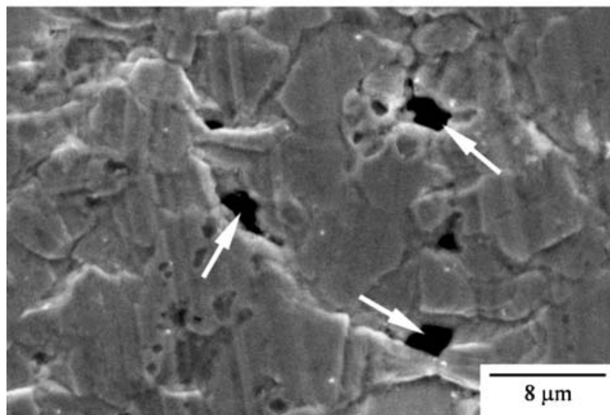

(b)

Figure 12 SEM micrographs of voids and microcracks (indicated by arrows) on the grain boundaries in creep specimens tested at RT: (a) Sn-3.5Ag and (b) Sn-3.5Ag-0.5Cu.

voids at IMCs, particularly on GBs, and their subsequent growth through a continuous creep deformation involving a dislocation creep mechanism, such as lattice diffusion-controlled dislocation climb, coupled with a dispersion-strengthening mechanism. This is supported by the fact that the rupture time data can be well described by the Monkman-Grant expression, which implied cavity formation and growth as the basic creep process [29]. In addition, when the testing temperature was increased from RT to 60 and 90 °C, the thermally activated dislocation movement would become more effective such that the stress exponent was decreased from 7 and 9 to 5 and 6, respectively, for Sn-3.5Ag and Sn-3.5Ag-0.5Cu. Note that the typical value of stress exponent for a type of lattice diffusion-controlled dislocation creep at high homologous temperatures (>0.4 T_m) in most metals is 5.

Igoshev *et al.* [6, 7] investigated the creep behavior of a Sn-3.5Ag alloy and found that the dispersed IMCs played two different roles. They may strengthen the matrix by acting as effective obstacles to dislocation motion and then prevent formation of large dislocation pileup at GBs. However, a higher number of precipitates in a given matrix, which generates more matrix/precipitate interfaces, is likely to cause more void/microcrack nucleation and accelerate the failure process. For the results obtained in the current study, an addition of 0.5 wt% of Cu into the Sn-3.5Ag alloy apparently gain more benefits from dispersion strengthening effect than the drawback of a higher likelihood of void/microcrack nucleation due to a slightly increased volume fraction of IMCs in the matrix. This is supported by the fact that at each given testing temperature, the Sn-3.5Ag-0.5Cu always has a higher stress exponent than does the Sn-3.5Ag.

4. Conclusions

(1) At a given temperature, both the Sn-3.5Ag and Sn-3.5Ag-0.5Cu alloys showed much better tensile and creep strength than the conventional Sn-37Pb solder due to a dispersion-strengthening mechanism.

(2) The greater creep rupture resistance of Sn-3.5Ag-0.5 Cu over Sn-3.5Ag in the temperature range from RT to 90 °C was attributable to a greater dispersion-strengthening effect by an addition of 0.5 wt% Cu and induced larger volume fraction of IMCs.

(3) The stress exponents of minimum strain rate were of 7 and 9 at RT and decreased to 5 and 6 at 60 and 90°C for the Sn-3.5Ag and Sn-3.5Ag-0.5Cu, respectively, suggesting the controlling creep mechanism for the given conditions was a lattice-controlled dislocation climb coupled with a dispersion-strengthening mechanism and the part of dispersion strengthening was more effective at a lower temperature.

(4) Fractography observations and measured stress exponents suggest that creep rupture of both lead-free solders occurred by the nucleation and growth of voids at IMCs on grain boundaries through a continuous creep deformation involving a dislocation creep mechanism, such as lattice diffusion-controlled dislocation climb, coupled with a dispersion strengthening mechanism.

(5) Both Monkman-Grant and Larson-Miller relationships were successfully applied to estimate the creep rupture time under various combinations of stress and temperature for each given lead-free alloy.

(6) By incorporation of Young's modulus to normalize the applied stress, the rupture time data at all given temperatures for each of the given binary and ternary Ag-containing solders could be well fitted by a simple power law with such a normalized stress term.

Acknowledgments

This work was supported by the National Science Council of the Republic of China (Taiwan) under Contract No. NSC 92-2216-E-008-007.

References

1. M. ABTEW and G. SELVADURAY, *Mater. Sci. Eng. R* **27** (2000) 95.
2. K. ZENG and K. N. TU, *ibid. R* **38** (2002) 55.
3. J. H. LAU, in "Solder Joint Reliability-Theory and Applications" (Van Nostrand Reinhold, New York, 1991).
4. M. OHRING, in "Reliability and Failure of Electronic Materials and Devices" (Academic Press, San Diego, CA, USA, 1998).
5. M. MCCORMACK, S. JIN, G. W. KAMMLOTT and H. S. CHEN, *Appl. Phys. Lett.* **63** (1993) 15.
6. V. I. IGOSHEV, J. I. KLEIMAN, D. SHANGGUAN, S. WONG and U. MICHON, *J. Electron. Mater.* **29** (2000) 1356.
7. V. I. IGOSHEV, J. I. KLEIMAN, D. SHANGGUAN, C. LOCK and S. WONG, *ibid.* **27** (1998) 1367.

8. W. J. PLUMBRIDGE, C. R. GAGG and S. PETERS, *ibid.* **30** (2001) 1178.
9. C. M. L. WU, D. Q. YU, C. M. T. LAW and L. WANG, *J. Mater. Res.* **17** (2002) 3146.
10. F. GUO, J. P. LUCAS and K. N. SUBRAMANIAN, *J. Mater. Sci.* **12** (2001) 27.
11. J. YU, D. K. JOO and S. W. SHIN, *Acta Mater.* **50** (2002) 4315.
12. D. K. JOO, J. YU and S. W. SHIN, *J. Electron. Mater.* **32** (2003) 541.
13. F. GUO, S. CHOI, K. N. SUBRAMANIAN, T. R. BIELER, J. P. LUCAS, A. ACHARI and M. PARUCHURI, *Mater. Sci. Eng. A* **351** (2003) 190.
14. K. WU, N. WADE, J. CUI and K. MIYAHARA, *J. Electron. Mater.* **32** (2003) 5.
15. H. G. SONG, J. W. MORRIS, JR. and F. HUA, *Mater. Trans.* **43** (2002) 1874.
16. M. L. HUANG and L. WANG, *J. Mater. Res.* **17** (2002) 2897.
17. N. WADE, K. WU, J. KUNII, S. YAMADA and K. MIYAHARA, *J. Electron. Mater.* **30** (2001) 1228.
18. H. MAVOORI, J. CHIN, S. VAYNMAN, B. MORAN, L. KEER and M. FINE, *ibid.* **26** (1997) 783.
19. M. E. LOOMANS and M. E. FINE, *Metall. Mater. Trans. A.* **31A** (2000) 1155.
20. K. W. MOON, W. J. BOETTINGER, U. R. KATTNER, F. S. BIANCANIELLO and C. A. HANDWERKER, *J. Electron. Mater.* **29** (2000) 1122.
21. A. K. MUKHERJEE, J. E. BIRD and J. E. DORN, *Trans. ASM* **62** (1969) 155.
22. H. J. FROST and M. F. ASHBY, in “Deformation-Mechanism Maps” (Pergamon Press, New York, 1982).
23. Z. MEI and J. W. MORRIS, JR., *J. Electron. Mater.* **21** (1992) 599.
24. S. W. SHIN and J. YU, *Jpn. Soc. Appl. Phys.* **42** (2003) 1368.
25. Z. MEI, D. GRIVAS, M. C. SHINE and J. W. MORRIS, JR., *J. Electron. Mater.* **19** (1990) 1273.
26. N. WADE, T. AKUZAWA, S. YAMADA, D. SUGIYAMA, I. KIM and K. MIYAHARA, *ibid.* **28** (1999) 1286.
27. F. C. MONKMAN and N. J. GRANT, *Proc. ASTM* **56** (1956) 593.
28. F. R. LARSON and J. MILLER, *Trans. ASME* **74** (1952) 765.
29. J. CADEK, in “Creep in Metallic Materials” (Elsevier Science Publishers, Amsterdam, The Netherlands, 1988).

Received 4 October 2004
and accepted 6 March 2005